Dynamical nucleus-nucleus potential and incompressibility of nuclear matter

V. Zanganeh,[1,2] N. Wang,[1,*] and O. N. Ghodsi[2]
[1]*Department of Physics, Guangxi Normal University, Guilin 541004, People's Republic of China*
[2]*Department of Physics, University of Mazandaran, Babolsar 47415, Iran*
(Received 9 January 2012; published 7 March 2012)

The dynamical nucleus-nucleus potentials for some fusion reactions are investigated by using the improved quantum molecular-dynamics (ImQMD) model with different sets of parameters in which the corresponding incompressibility coefficient of nuclear matter is different. Two new sets of parameters SKP* and IQ3 for the ImQMD model are proposed with the incompressibility coefficient of 195 and 225 MeV, respectively. The measured fusion excitation function for ^{16}O+^{208}Pb and the charge distribution of fragments for Ca+Ca and Au+Au in multifragmentation process can be reasonably well reproduced. Simultaneously, the influence of the nuclear matter incompressibility and the range of nucleon-nucleon interaction on the nucleus-nucleus dynamic potential is investigated.

DOI: 10.1103/PhysRevC.85.034601 PACS number(s): 25.70.−z, 21.65.Mn, 24.10.Cn

I. INTRODUCTION

The synthesis of superheavy nuclei and heavy-ion fusion at deep sub-barrier energies has attracted a great deal of attention in recent years [1–8]. The calculation of nucleus-nucleus potential especially at short distances is of crucial importance for these studies. Several static and dynamic models have been proposed for calculating the nucleus-nucleus potential [9–15]. The static potentials are usually obtained by some empirical formulas or based on the double-folding concept and the sudden approximation. To consider the dynamical process in fusion reaction microscopically, some microscopic dynamics models, such as the time-dependent Hartree-Fock (TDHF) model [13,14] and the improved quantum molecular dynamic (ImQMD) model [16,17] have been developed. The ImQMD model is a semiclassical microscopic dynamics model and is successfully applied on intermediate-energy heavy-ion collisions and heavy-ion reactions at energies around the Coulomb barrier [15,17,18]. In Ref. [15] the extended Thomas-Fermi approximation is adopted for calculation of the dynamical nucleus-nucleus potential at short distances based on the obtained dynamical densities of the reaction system from the ImQMD simulations. The energy dependence of the dynamical nucleus-nucleus potential was observed. In addition to the influence of the incident energy on the nucleus-nucleus potential due to the dynamical evolution of the densities, the influence of the incompressibility coefficient of nuclear matter on the nucleus-nucleus potential and the fusion cross sections are also investigated in Refs. [19,20] according to the double-folding calculation with the M3Y interactions.

To investigate the influence of nuclear equation of state on the dynamical nucleus-nucleus potential, we will study the nucleus-nucleus potential at short distances with the ImQMD model by adopting different sets of parameters. The corresponding nuclear equation of state for these different sets of parameters is different, with which we attempt to understand the influence of the incompressibility coefficient of nuclear matter on the dynamical fusion potential. The structure of this paper is as follows: In Sec. II, the ImQMD model is briefly introduced. In Sec. III, two sets of parameters IQ3 and SKP* are proposed for the ImQMD calculation, and the fusion reactions ^{16}O+^{208}Pb and ^{48}Ca+^{208}Pb at energies around the Coulomb barrier and the reactions Ca+Ca and Au+Au at incident energy of 35MeV/nucleon are also studied for testing IQ3 and SKP*. In addition, the dynamical nucleus-nucleus potential inside the Coulomb barrier is simultaneously investigated. Finally the conclusion is given in Sec. IV.

II. IMPROVED QUANTUM MOLECULAR-DYNAMICS MODEL

In the ImQMD model, as in the original QMD model [21], each nucleon is represented by a coherent state of a Gaussian wave packet. The density distribution function ρ of a system reads

$$\rho(\mathbf{r}) = \sum_i \frac{1}{\left(2\pi\sigma_r^2\right)^{3/2}} \exp\left[-\frac{(\mathbf{r}-\mathbf{r}_i)^2}{2\sigma_r^2}\right], \tag{1}$$

where σ_r represents the spatial spread of the wave packet. The propagation of nucleons is governed by Hamiltonian equations of motion under the self-consistently generated mean field,

$$\dot{\mathbf{r}}_i = \frac{\partial H}{\partial \mathbf{p}_i}, \quad \dot{\mathbf{p}}_i = -\frac{\partial H}{\partial \mathbf{r}_i}, \tag{2}$$

where r_i and p_i are the center of the ith wave packet in the coordinate and momentum space, respectively. The Hamiltonian H consists of the kinetic energy $T = \sum_i \frac{\mathbf{p}_i^2}{2m}$ and the effective interaction potential energy U:

$$H = T + U. \tag{3}$$

The effective interaction potential energy is written as the sum of the nuclear interaction potential energy $U_{\rm loc} = \int V_{\rm loc}(\mathbf{r})d\mathbf{r}$ and the Coulomb interaction potential energy $U_{\rm Coul}$, which includes the contribution of the direct and exchange terms,

$$U = U_{\rm loc} + U_{\rm Coul}. \tag{4}$$

*wangning@gxnu.edu.cn

TABLE I. Model parameters adopted in this work.

Parameter	α (MeV)	β (MeV)	γ	$g_{\rm sur}$ (MeVfm^2)	g_τ (MeV)	η	C_s (MeV)	κ_s (fm^2)	ρ_0 (fm^{-3})	σ_0 (fm)	σ_1 (fm)
IQ2	−356	303	7/6	7.0	12.5	2/3	32.0	0.08	0.165	0.88	0.09
SKP*	−356	303	7/6	19.5	13.0	2/3	35.0	0.65	0.162	0.94	0.018
IQ3	−207	138	7/6	18.0	14.0	5/3	32.0	0.08	0.165	0.94	0.018

$V_{\rm loc}(r)$ is the potential-energy density that is obtained from the effective Skyrme interaction and taken to be the same as that in Ref. [17]:

$$V_{\rm loc} = \frac{\alpha}{2}\frac{\rho^2}{\rho_0} + \frac{\beta}{\gamma+1}\frac{\rho^{\gamma+1}}{\rho_0^{\gamma}} + \frac{g_{\rm sur}}{2\rho_0}(\nabla\rho)^2 + g_\tau\frac{\rho^{\eta+1}}{\rho_0^{\eta}} + \frac{C_s}{2\rho_0}[\rho^2 - k_s(\nabla\rho)^2]\delta^2, \quad (5)$$

where $\delta = (\rho_n - \rho_p)/(\rho_n + \rho_p)$ is the isospin asymmetry. To describe the fermionic nature of the N-body system and to improve the stability of an individual nucleus, the phase-space occupation constraint method [22] and the system-size-dependent wave-packet width $\sigma_r = \sigma_0 + \sigma_1 A^{1/3}$ fm [16] are adopted. The parameter sets adopted in this work are shown in Table I.

III. RESULTS

In this section we first briefly introduce the parameter sets IQ3 and SKP*. Then we test the new parameter sets through fusion reactions and heavy-ion collisions at intermediate energy. Finally we investigate the dynamical nucleus-nucleus potential inside of the Coulomb barrier.

A. New parameter sets SKP* and IQ3

According to the properties of nuclei at ground state and the knowledge of nuclear incompressibility, a number of Skyrme forces, such as SkM* [23], SKP [24], and SLy4 [25], were proposed in recent decades. With the proposed parameter sets, the Skyrme energy-density functionals have been successfully applied on the studies of nuclear structure, fusion reaction, and neutron star, etc. Based on the parameters of Skyrme forces, the ImQMD parameters can be directly obtained as those done in Ref. [18]. Considering the range of nucleon-nucleon interaction in the ImQMD model, which is represented by a gaussian wave packet, the parameters of the ImQMD model in this work are re-adjusted for studying the fusion reactions in which the stability of an individual nucleus plays a role for a reliable description of the dynamical process.

The knowledge of nuclear equation of state at densities around the normal density ρ_0 is helpful to constrain the model parameters. In the ImQMD model, the incompressibility coefficient K_∞ of symmetric nuclear matter at ρ_0 is expressed as

$$K_\infty = 9\rho_0^2\frac{\partial^2(E/A)}{\partial\rho^2}\bigg|_{\rho=\rho_0} = -2\xi c_k\rho_0^{2/3} + 9\beta(\gamma-1)\gamma + 9g_\tau(\eta-1)\eta \quad (6)$$

with $c_k = \frac{\hbar^2}{2m}\frac{3}{5}(\frac{3\pi^2}{2})^{2/3} = 75.0$ MeV fm^2. $\xi = c_0/c_k$ is a correction factor for the kinetic energy of a nuclear system when applying the extended Thomas-Fermi (ETF) approximation, which is roughly expressed as

$$E_k^{\rm ETF} \simeq c_0\sum_i \rho_i^{2/3} + \frac{c_1}{\sum\rho_i}\sum_{i,j\neq i} f_s\rho_{ij} + c_2 N \quad (7)$$

in this model. The expressions of ρ_i and ρ_{ij} are given in Ref. [15]. The coefficients c_0, c_1, and c_2 can be determined by the kinetic energies T of nuclei at their ground state. $\xi = 1$ is for the idealistic Fermi gas. Considering the range of realistic nucleon-nucleon interactions, which is described by gaussian wave packets in the ImQMD model, we approximately set $\xi = 0.4 \sim 0.6$ for a reasonable description of the properties of nuclei at ground state and the stability of an individual nucleus. The corresponding energy per particle E/A at ρ_0 reads

$$\frac{E(\rho)}{A}\bigg|_{\rho=\rho_0} = \xi c_k\rho_0^{2/3} + \frac{\alpha}{2} + \frac{\beta}{\gamma+1} + g_\tau. \quad (8)$$

Although experimental and theoretical investigations on the nuclear equation of state suggest that $K_\infty \approx 230$ MeV, $E/A \approx -16$ MeV around the saturation density which is $\sim$0.16 fm^{-3} [26–28], the uncertainty of nuclear equation of state still causes some difficulties for an unambiguous determination of the model parameters.

To investigate the influence of the nuclear matter incompressibility coefficient on fusion reactions, we attempt to propose two new sets of parameters, SKP* and IQ3 for the ImQMD simulations. The parameter set SKP* is generally determined based on the Skyrme force SKP [24] in which the parameters g_τ, σ_0, and σ_1 are adjusted for an appropriate description of nuclear properties at ground state and the fusion reactions. For both IQ2 and SKP*, the corresponding values of K_∞ are the same but the wave-packet widths σ_r are different, which is useful for exploring the influence of the interaction range of nucleons and the finite-size effect of nuclei. To explore the influence of the nuclear matter incompressibility on the fusion reactions, we also construct the parameter set IQ3 in which the wave-packet widths σ_r are the same as those in SKP* but the incompressibility coefficient $K_\infty = 225$ MeV is obviously larger than that in SKP* and IQ2 (see Table II). The corresponding kinetic-energy coefficients for different sets of parameters are listed in Table II.

B. Tests for IQ3 and SKP*

With the parameter sets IQ3 and SKP*, the time evolutions of the binding energies and nuclear radii for a number of nuclei have been checked. We find that an individual nucleus

TABLE II. Kinetic-energy coefficients in the ETF approximation and incompressibility coefficient for parameter sets IQ2, SKP*, and IQ3.

Parameter	c_0 (MeV fm^2)	c_1 (MeV fm^2)	c_2 (MeV)	K_∞ (MeV)
IQ2	41.2	4.8	−1.0	195
SKP*	38.9	0.1	0	195
IQ3	43.3	0.34	0	225

can remain stable for several thousands fm/c without spurious nucleon emission. Simultaneously, some fusion reactions are investigated for testing the parameter sets. Figure 1 shows the time evolution of the densities for the fusion reaction ^{48}Ca+^{208}Pb at an incident energy of $E_{\rm c.m.} = 200$ MeV with the parameter set IQ3. From the time evolution, one sees that the central densities of nuclei in the reactions are reasonable. In addition, we note that the surface diffuseness of nuclei at the neck region increases when the neck of the dinuclear system is well formed.

The fusion cross sections of ^{16}O+^{208}Pb are also calculated with the ImQMD model by adopting IQ3 and SKP*. Through creating certain bombarding events (about 100) at each incident energy $E_{\rm c.m.}$ and at each impact parameter b, and counting the number of fusion events, we obtain the fusion probability $g_{\rm fus}(E_{\rm c.m.}, b)$ of the reaction, by which the fusion cross section can be calculated [16]:

$$\sigma_{\rm fus}(E_{\rm c.m.}) = 2\pi \int b\, g_{\rm fus}\, db \simeq 2\pi \sum b\, g_{\rm fus}\, \Delta b. \qquad (9)$$

The initial distance between the projectile and target is taken to be $R = 40$ fm for calculating the fusion cross sections. Figure 2 shows the comparison of our calculated results and the experimental data for the fusion reaction ^{16}O+^{208}Pb. The solid and open circles denote the experimental data and the calculation results, respectively. The measured fusion excitation function for ^{16}O+^{208}Pb can be reasonably well reproduced with the new parameter set IQ3 and SKP* at energies near and above the Coulomb barrier. The overprediction of the fusion cross sections at sub-barrier energies is due to the shell effect of doubly magic nuclei that is not well described with this semiclassical model.

For further testing the reliability of IQ3 and SKP*, we have also calculated the charge distributions of fragments in multifragmentation processes at intermediate energy heavy-ion collisions. In Fig. 3 we show the charge distribution of fragments by using the ImQMD model with parameters set of IQ3 and SKP* for ^{40}Ca+^{40}Ca [30] and ^{197}Au+^{197}Au [31] at incident energy of 35 MeV/nucleon. Here we create 500 events for head-on collisions and for each event we self-consistently simulate the whole collision process until $t = 6000$ fm/c with a step size of $\Delta t = 1$ fm/c. We have found that the experimental data can be reproduced remarkably well.

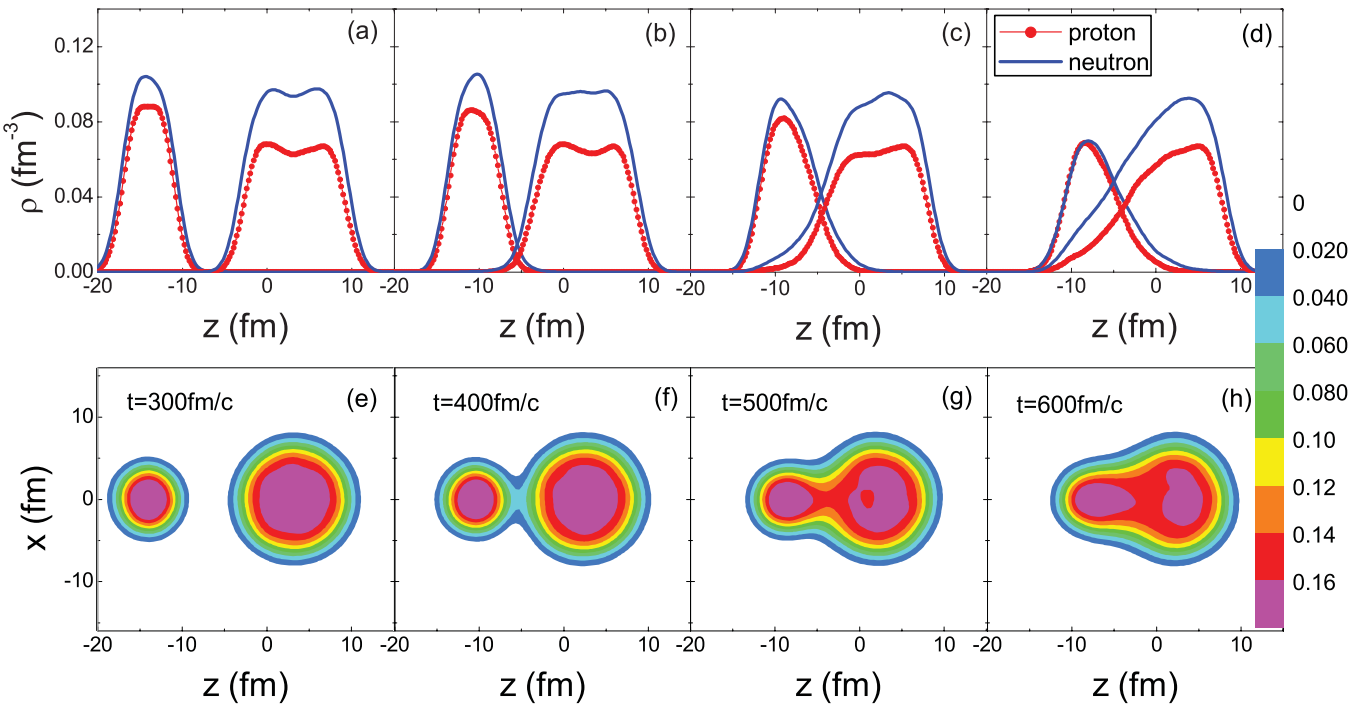

FIG. 1. (Color online) Time evolution of the density distribution for the fusion reaction ^{48}Ca+^{208}Pb at an incident energy of $E_{\rm c.m.} = 200$ MeV with IQ3.

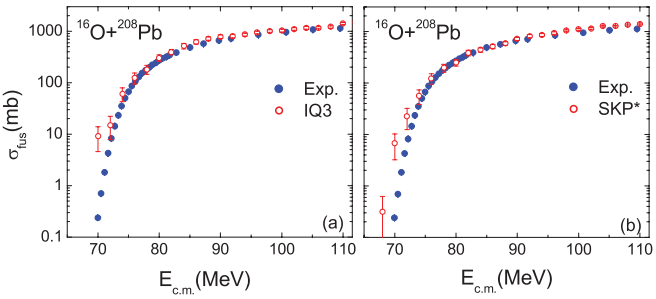

FIG. 2. (Color online) Fusion excitation function of ^{16}O+^{208}Pb reaction. The solid circles denote the experimental data [29]. The open circles denote the results of ImQMD with parameter sets IQ3 and SKP*.

C. Dynamical nucleus-nucleus potential

Based on the dynamical densities of the reaction system, the nucleus-nucleus potential can be obtained with the ETF approximation for the kinetic energies [15]. After the dinuclear system is formed, the nucleus-nucleus potential may be described by a way like the entrance channel potential [10]

$$V(R) = E_{\rm tot}(R) - \bar{E}_1 - \bar{E}_2, \tag{10}$$

where $E_{\rm tot}(R)$ is the energy of the composite system, which is strongly dependent on the dynamical density distribution of the system obtained with the ImQMD model, $\bar{E}_1$ and $\bar{E}_2$ are the time average of the energies of the projectile and target nuclei, respectively. In this work, the dynamical nucleus-nucleus potential is calculated the same as in Ref. [15], but with the parameter sets IQ3 and SKP*. The kinetic-energy coefficients c_0, c_1, and c_2 listed in Table II are determined by

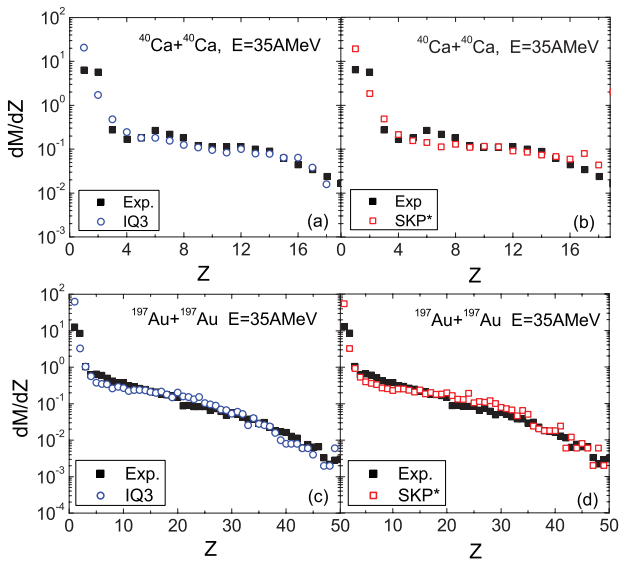

FIG. 3. (Color online) Charge distribution of fragments for central collision of ^{197}Au+^{197}Au and ^{40}Ca+^{40}Ca at 35 A MeV. The solid squares denote the experimental data taken from Refs. [30,31]. The open circles and open squares denote the results of ImQMD with IQ3 and SKP*, respectively.

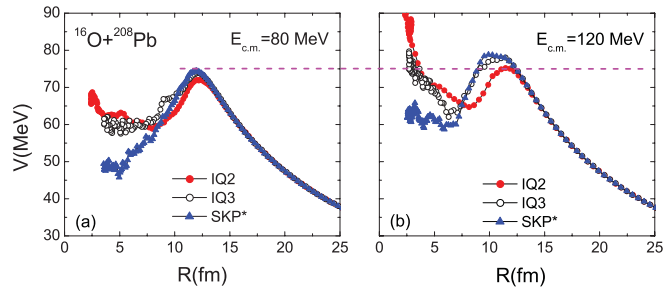

FIG. 4. (Color online) Dynamical nucleus-nucleus potential for the reaction ^{16}O+^{208}Pb with parameter set IQ2, IQ3, and SKP* at incident energies of (a) $E_{\rm c.m.} = 80$ MeV and (b) $E_{\rm c.m.} = 120$ MeV, respectively. Here we set the initial distance between two nuclei as 30 fm. The solid circles, open circles, and triangles denote the results with IQ2, IQ3, and SKP*, respectively. The dashed line is to guide the eyes.

fitting the obtained kinetic energies T of a series of nuclei from light to heavy nuclei at their ground state with Eq. (7). To investigate the dynamical nucleus-nucleus potential, the head-on collisions of ^{16}O+^{208}Pb and ^{48}Ca+^{208}Pb at two different incident energies with three different parameter sets have been studied. As mentioned previously, the values of the incompressibility coefficient are the same but the wave-packet widths are different for IQ2 and SKP*, while the incompressibility coefficients are different but the wave-packet widths are the same for IQ3 and SKP*.

Figures 4 and 5 show the dynamical nucleus-nucleus potential for ^{16}O+^{208}Pb and ^{48}Ca+^{208}Pb with the parameter sets IQ2, IQ3, and SKP*, respectively. From the figures we find that (1) the dynamical barrier height depends on the incident energy as mentioned in Ref. [15], (2) the wave-packet width influences nuclear surface diffuseness and thus influences both the potential barrier height and the potentials at short distances, and (3) the nuclear matter incompressibility seems just to affect the potentials at short distances if taking the same wave-packet width. Comparing the results with SKP* and IQ3, one sees that the potentials at short distances increase with the increase of the incompressibility coefficient. To illustrate this point, we also study the static entrance channel potential [10] of ^{48}Ca+^{208}Pb with the Skyrme energy-density function by adopting different parameter sets. Figure 6 shows the nuclear potential (i.e., removing the Coulomb potential

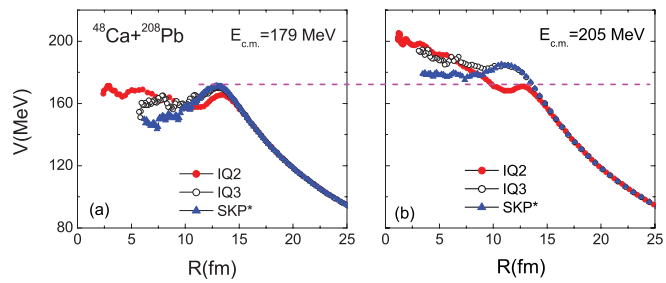

FIG. 5. (Color online) The same as Fig. 4, but for the reaction ^{48}Ca+^{208}Pb at incident energies of (a) $E_{\rm c.m.} = 179$ MeV and (b) $E_{\rm c.m.} = 205$ MeV, respectively.

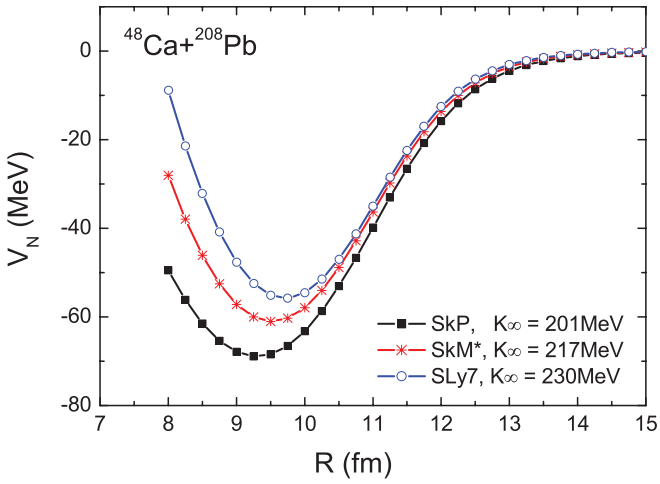

FIG. 6. (Color online) Nuclear potential of ^{48}Ca+^{208}Pb with different Skyrme forces. The solid squares, stars, and open circles denote the results with SKP, SkM*, and SLy7, respectively.

from the entrance channel nucleus-nucleus potential) as a function of distance between two nuclei. Obviously, the nuclear potentials do increase with the value of K_∞. In addition, the obtained dynamical nucleus-nucleus potential has been checked by directly using the barrier penetration calculations for the fusion cross section. As an example, the fusion cross section for the reaction ^{16}O+^{208}Pb at $E_{\rm c.m.} = 80$ MeV is calculated based on the obtained potential for head-on collisions with IQ3, which is shown in Fig. 4(a). We find that the obtained fusion cross section with the barrier penetration approach is very close to the result with Eq. (9). We also note that the obtained fusion probability $g_{\rm fus}$ in central and peripheral collisions is different with the two approaches for this reaction. The difference is due to that the reduced mass μ in the traditional barrier penetration calculations is fixed, but it changes as a function of distance R between two nuclei in the ImQMD simulations when the neck of the composite system is formed.

TABLE III. The same as Table II, but taking different value for β.

Parameter	c_0 (MeV fm^2)	c_1 (MeV fm^2)	K_∞ (MeV)
$\beta = 138$	43.3	0.34	225
$\beta = 140$	40.8	0.30	229
$\beta = 142$	38.0	0.83	232
$\beta = 145$	33.8	1.43	237

To further investigate the influence of nuclear repulsion on the nucleus-nucleus potential, we study the nucleus-nucleus potential with IQ3 but varying the parameter β. The value of β and the corresponding kinetic-energy coefficients and K_∞ are listed in Table III (here $c_3 = 0$). Figure 7 shows the dynamical nucleus-nucleus potential and the contribution of the corresponding effective interaction potential energy and that of the corresponding kinetics energy for the reaction ^{16}O+^{208}Pb with different values of β. One can see from Fig. 7(b) that the contribution of the effective interaction potential energy increases with the nuclear incompressibility coefficient as we expected. But we also note that the change of β causes larger change of the corresponding kinetic energy than that of the interaction potential energy, which results in the decrease of the total nucleus-nucleus potential at short distances with increasing the nuclear repulsion.

IV. CONCLUSION

In this work, the dynamical nucleus-nucleus potentials for fusion reactions have been investigated by using the improved quantum molecular-dynamics model with different sets of parameters. By using two new sets of parameters IQ3 and SKP* with which the measured fusion excitation function for ^{16}O+^{208}Pb and the charge distribution of fragments for Ca+Ca and Au+Au in multifragmentation process can be reasonably well reproduced, we find that both the nuclear incompressibility and the range of nucleon-nucleon interactions significantly influence the nucleus-nucleus potential. The

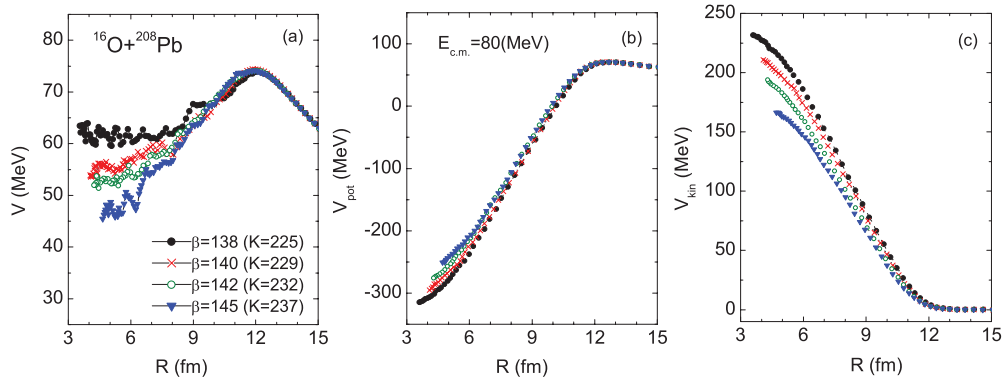

FIG. 7. (Color online) (a) Dynamical nucleus-nucleus potential, (b) contribution of the interaction potential energy, and (c) contribution of the kinetics energy for reaction ^{16}O+^{208}Pb at $E_{\rm c.m.} = 80$ MeV based on the parameter set IQ3 but varying the value of β. The solid circles, crosses, open circles, and triangles denote the results with $\beta = 138$, 140, 142, and 145 MeV, respectively.

interaction range represented by the gaussian wave-packet width affects both the barrier height and the potentials at short distances. The incompressibility coefficient of nuclear matter mainly influences the potentials at short distances if taking the same wave-packet width. In addition, the nuclear repulsion influences both the effective interaction potential energy and the kinetic energy of a fusion system.

ACKNOWLEDGMENTS

This work was supported by National Natural Science Foundation of China, Grants No. 10875031, No. 11005003, and No. 10979024. One of the authors (V.Z.) acknowledges support from the General Department of Scholarships and Student Affairs, Ministry of Science and Technology, Iran.

[1] S. Hofmann and G. Münzenberg, Rev. Mod. Phys. **72**, 733 (2000).
[2] Yu. Ts. Oganessian *et al.*, Phys. Rev. Lett. **104**, 142502 (2010).
[3] V. Zagrebaev and W. Greiner, Phys. Rev. C **78**, 034610 (2008).
[4] G. G. Adamian, N. V. Antonenko, A. Diaz-Torres, and W. Scheid, Nucl. Phys. A **671**, 233 (2000).
[5] B. N. Lu, E. G. Zhao, and S. G. Zhou, Phys. Rev. C **85**, 011301(R) (2012).
[6] N. Wang, J. Tian, and W. Scheid, Phys. Rev. C **84**, 061601(R) (2011).
[7] V. V. Sargsyan, G. G. Adamian, N. V. Antonenko, W. Scheid, and H. Q. Zhang, Phys. Rev. C **84**, 064614 (2011).
[8] H. Timmers, D. Ackermann, S. Beghini, and N. Rowley, Nucl. Phys. A **633**, 421 (1998).
[9] W. D. Myers and W. J. Swiatecki, Phys. Rev. C **62**, 044610 (2000).
[10] M. Liu, N. Wang, Z. Li, X. Wu, and E. Zhao, Nucl. Phys. A **768**, 80 (2006).
[11] N. Wang, K. Zhao, W. Scheid, and X. Wu, Phys. Rev. C **77**, 014603 (2008).
[12] O. N. Ghodsi and V. Zanganeh, Phys. Rev. C **79**, 044604 (2009).
[13] A. S. Umar and V. E. Oberacker, Phys. Rev. C **74**, 021601(R) (2006).
[14] A. S. Umar, V. E. Oberacker, J. A. Maruhn, and P. G. Reinhard, Phys. Rev. C **85**, 017602 (2012).
[15] Y. Jiang, N. Wang, Z. Li, and W. Scheid, Phys. Rev. C **81**, 044602 (2010).
[16] N. Wang, Z. Li, and X. Wu, Phys. Rev. C **65**, 064608 (2002).
[17] N. Wang, Z. Li, X. Wu, J. Tian, Y. X. Zhang, and M. Liu, Phys. Rev. C **69**, 034608 (2004).
[18] Y. Zhang and Z. Li, Phys. Rev. C **74**, 014602 (2006).
[19] S. Misicu and H. Esbensen, Phys. Rev. C **75**, 034606 (2007).
[20] O. N. Ghodsi and V. Zanganeh, Nucl. Phys. A **846**, 40 (2010).
[21] J. Aichelin, Phys. Rep. **202**, 233 (1991).
[22] M. Papa, T. Maruyama, and A. Bonasera, Phys. Rev. C **64**, 024612 (2001).
[23] J. Bartel, P. Quentin, M. Brack, C. Guet, and H.-B. Hakansson, Nucl. Phys. A **386**, 79 (1982).
[24] J. Dobaczewski, H. Flocard, and J. Treiner, Nucl. Phys. A **422**, 103 (1984).
[25] E. Chabanat, P. Bonche, P. Haensel, J. Meyer, and R. Schaeffer, Nucl. Phys. A **635**, 231 (1998).
[26] Y. W. Lui, D. H. Youngblood, Y. Tokimoto, H. L. Clark, and B. John, Phys. Rev. C **70**, 014307 (2004).
[27] U. Garg *et al.*, Nucl. Phys. A **788**, 36 (2007).
[28] C. Fuchs, Prog. Part. Nucl. Phys. **56**, 1 (2006)
[29] C. R. Morton, A. C. Berriman, M. Dasgupta, D. J. Hinde, J. O. Newton, K. Hagino, and I. J. Thompson, Phys. Rev. C **60**, 044608 (1999).
[30] K. Hagel *et al.*, Phys. Rev. C **50**, 2017 (1994).
[31] P. Dsesquelles *et al.*, Nucl. Phys. A **633**, 547 (1998).